Expanded View Figures

Figure EV1. The TOLLIP C2, IDR, and CUE domains are required for degradation of an aberrant ER membrane protein.

A Lysosomal degradation of A53T-HP in HEK293A cells transfected with indicated siRNAs and mCherry-A53T-HP. The graph represents mean ± SEM of mCherry processing ($n = 4$ independent experiments).

B As in (A), but HeLa cells were used.

C Immunofluorescence of HEK293A cells transfected with mCherry-EGFP-A53T-HP and stained with an anti-RAB7 antibody. Scale bars, 10 and 2 μm (insets) ($n = 3$ independent experiments).

D The effect of TOLLIP overexpression on lysosomal degradation of cytosolic A53T α-synuclein, ER membrane protein E-Syt1, and A53T-HP. HEK293A cells were transfected with indicated mCherry-tagged constructs and FLAG-TOLLIP. Numerical data represent mean ± SEM of TOLLIP-dependent fold change in mCherry processing for each mCherry-tagged construct ($n = 3$ independent experiments).

E, F Turnover of A53T-HP monitored by promoter shut-off assay. HEK293A cells were transfected with HA-tagged mCherry-A53T-HP harboring a tetracycline (Tet)-responsive promoter, Tet repressor, and FLAG-TOLLIP variants. Cells were treated with 0.5 μg/ml Tet for 24 h to induce the expression of mCherry-A53T-HP and then replenished with fresh medium without Tet to allow for RNA decay. Twenty-four hours after Tet washout was set to time 0, and the remaining mCherry-A53T-HP protein expression level was evaluated at indicated time points. The graphs represent mean ± SEM of the turnover of mCherry-A53T-HP protein quantified by immunoblotting and RNA quantified by real-time quantitative PCR in parallel experiments to confirm comparable clearance of the transcripts in all conditions ($n = 3$ independent experiments). Statistical significance was determined at the final time points. ΔTBD, Δ1–44; $C2^{mut\ \#1}$, R123A; IDR^{mut}, 181–229 > $(GGGGS)_9GGGG$; ΔIDR, Δ181–229; CUE^{mut}, L267A and L268A; LIR^{mut}, W133A, T134A, H135A, I136A, W151A, Y152A, S153A, and L154A.

Data information: $*P < 0.05$, $**P < 0.01$, $***P < 0.001$ by one-way ANOVA with Dunnett's multiple comparison test (A, B, E and F).

© 2023 The Authors

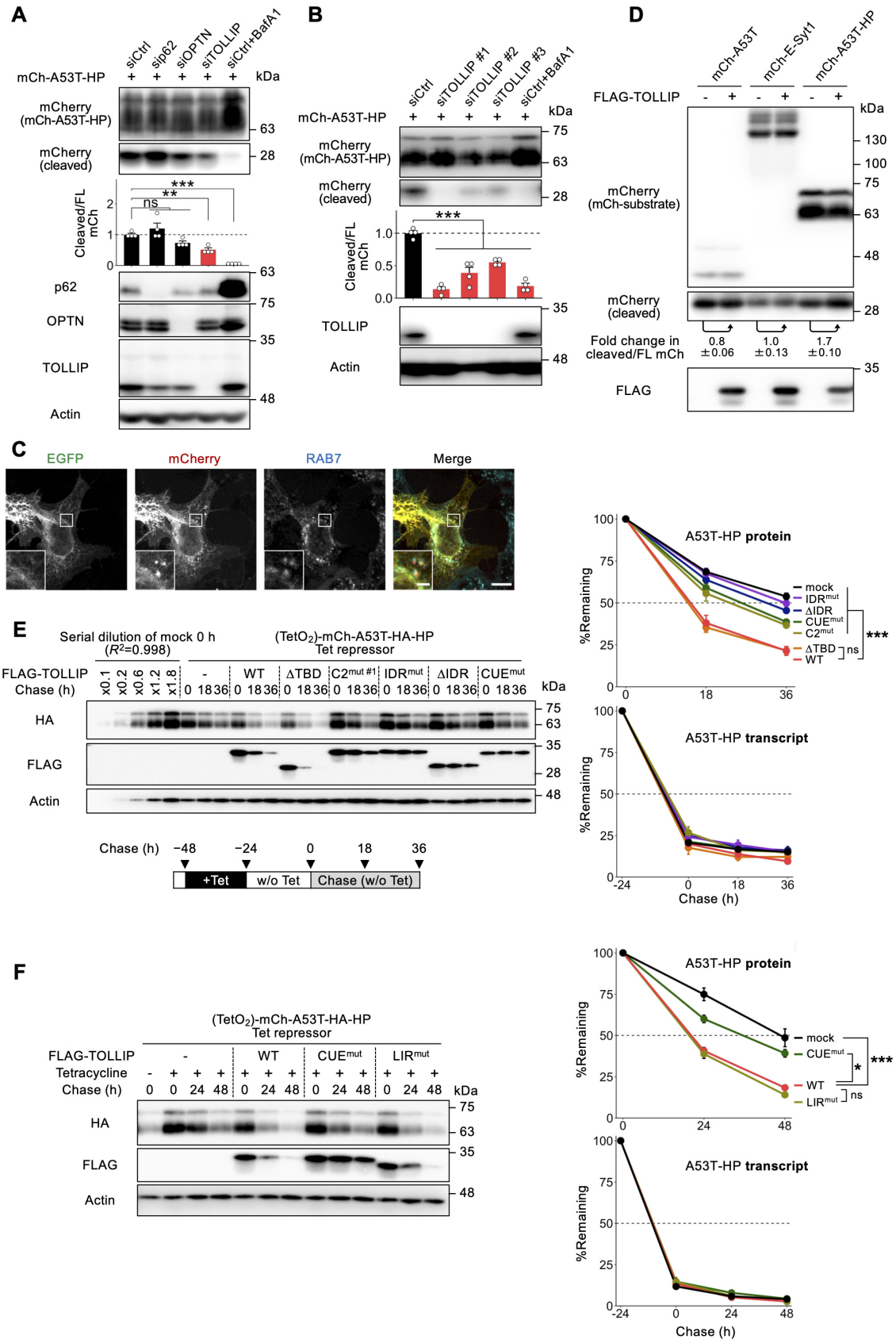

Figure EV1.

© 2023 The Authors

Figure EV2. Ubiquitination enhances lysosomal degradation of an aberrant ER membrane protein.

A Co-IP of FLAG-TOLLIP variants with endogenous ubiquitin conjugates. HEK293A cells were transfected with FLAG-TOLLIP variants and lysed in buffers containing 1% Triton X-100 (TX-100) or 0.1% SDS (RIPA). Co-IP was performed with an anti-FLAG antibody. Since ubiquitin conjugates coimmunoprecipitated from RIPA lysates can be regarded as those covalently attached to TOLLIP, the differences in the amount of ubiquitin conjugates in the TX-100 lysed and RIPA lysed fractions were regarded as ubiquitinated endogenous proteins complexed with TOLLIP. The graph represents mean ± SEM of these differences ($n = 3$ independent experiments).

B *In vitro* binding assay of HSP70 and heat-denatured luciferase. Recombinant GST fusion proteins were incubated with recombinant luciferase at 4 or 42°C for 120 min and purified using glutathione Sepharose. The data are representative of four experiments performed with the same batches of purified proteins.

C Denaturing IP to evaluate the expression level of ubiquitinated A53T-HP. HEK293A cells were transfected with indicated siRNAs and HA-tagged mCherry-A53T-HP, treated with or without 100 nM BafA1 for 20 h, and lysed under denaturing conditions. The lysates were subjected to IP using an anti-HA antibody. The graph represents mean ± SEM of the BafA1-dependent fold increase in the amount of ubiquitinated species (top panel) normalized to unmodified species (second panel) ($n = 3$ independent experiments).

D Lysosomal degradation of A53T-HP in HEK293A cells transfected with FLAG-NEDD4 WT or catalytically inactive C867S (CS) and mCherry-A53T-HP. The graph represents mean ± SEM of mCherry processing ($n = 3$ independent experiments). In parallel, the cells were lysed under either nondenaturing or denaturing conditions and subjected to IP with an anti-HA antibody to evaluate the interaction of A53T-HP with NEDD4 or the ubiquitination status of A53T-HP, respectively. Although the C867S mutation in the catalytic core diminishes NEDD4 E3 activity, the mutant retained substrate-binding capacity, possibly because distal WW domains recognized α-synuclein (Tofaris *et al*, 2011).

Data information: $*P < 0.05$, $**P < 0.01$, $***P < 0.001$ by one-way ANOVA with Dunnett's multiple comparison test (C and D).

© 2023 The Authors

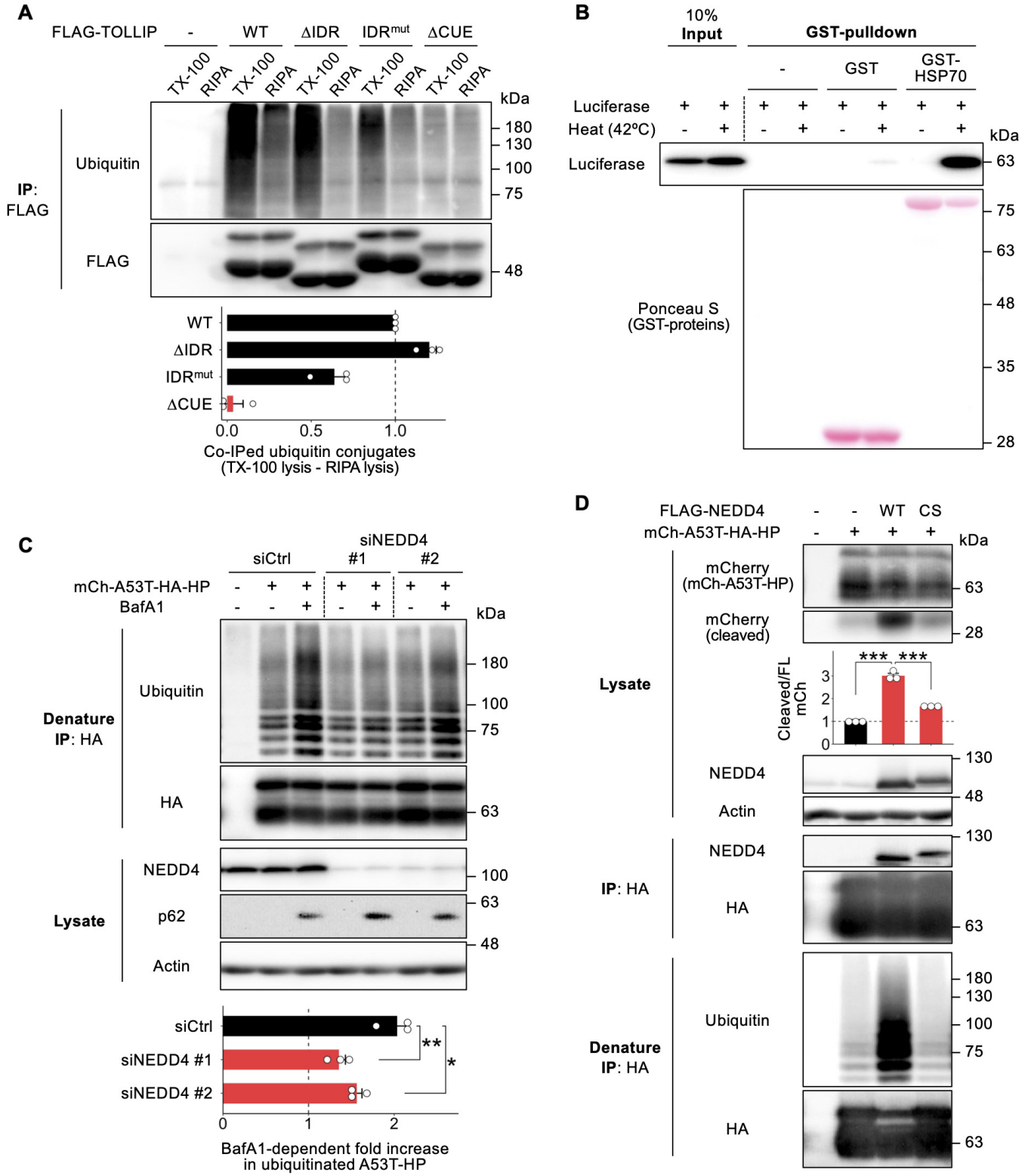

Figure EV2.

© 2023 The Authors

Figure EV3. TOLLIP promotes PI3P-dependent lysosomal trafficking of an aberrant ER membrane protein.

A Fluorescence microscopy imaging to monitor the lysosomal delivery of A53T-HP. HEK293A cells were transfected with indicated siRNAs and constructs, treated with 100 nM BafA1 with or without 0.5 μM SAR405 for 12 h, and stained with an anti-FLAG antibody. The percentage of LAMP1 puncta containing mCherry-A53T-HP in each cell was quantified. From 12 to 26 cells in each condition pooled from $n = 2$ independent experiments were analyzed. Scale bars, 10 and 2 μm (insets).

B Validation of the loss of VPS34 function in an experiment conducted in parallel with (A) except for BafA1 treatment ($n = 2$ independent experiments).

C Another example of CLEM images as in Fig 4E. Serial 50 nm sections are shown. Black arrowhead indicates a single membrane surrounding a vesicle and white arrowheads indicate a smooth ER-like double-membrane structure located in close proximity to the vesicle. N, nucleus; M, mitochondria. Scale bars, 500 and 50 nm (inset).

D Turnover of A53T-HP monitored by promoter shut-off assay in HEK293A cells transfected with indicated plasmids as in Fig EV1E and F. The graph represents mean ± SEM of the turnover of mCherry-A53T-HP protein ($n = 3$ independent experiments).

E Fractionation into the postnuclear membrane (P100) and the cytosol (S100) of HEK293A cells transfected with Venus-TOLLIP and mCherry-A53T-HP and treated with or without 10 μM SAR405 for 24 h. In parallel, whole-cell lysates (WCLs) were prepared to confirm TOLLIP- and PI3P-dependent lysosomal degradation of A53T-HP under these experimental conditions ($n = 3$ independent experiments).

F Lysosomal degradation of A53T-HP in parental or *CCPG1*-KO HEK293A cells transfected with indicated siRNAs and mCherry-A53T-HP. The graph represents mean ± SEM of mCherry processing ($n = 6$ independent experiments).

G Validation of macroautophagy-defective HEK293A cell lines. Cells with indicated genotypes were treated with or without the macroautophagy inducer 1 μM rapamycin for 7 h and 200 nM BafA1 for 4 h. Impaired LC3-II flux (BafA1-dependent increase in the LC3-II level) and p62 accumulation suggest that macroautophagy is defective in *FIP200*-KO and *ATG7*-KO cells ($n = 2$ independent experiments).

H Lysosomal degradation of A53T-HP in parental or *FIP200*-KO HEK293A cells transfected with indicated constructs. The graph represents mean ± SEM of mCherry processing ($n = 3$ independent experiments).

I Turnover of A53T-HP monitored by promoter shut-off assay in HEK293A cells with indicated genotypes as in (D). The graph represents mean ± SEM of the turnover of mCherry-A53T-HP protein ($n = 3$ independent experiments).

Data information: $*P < 0.05$, $**P < 0.01$, $***P < 0.001$ by one-way ANOVA with Dunnett's (D and I) or Tukey's (F) multiple comparison test or unpaired two-tailed Student's *t* test (A and H).

© 2023 The Authors

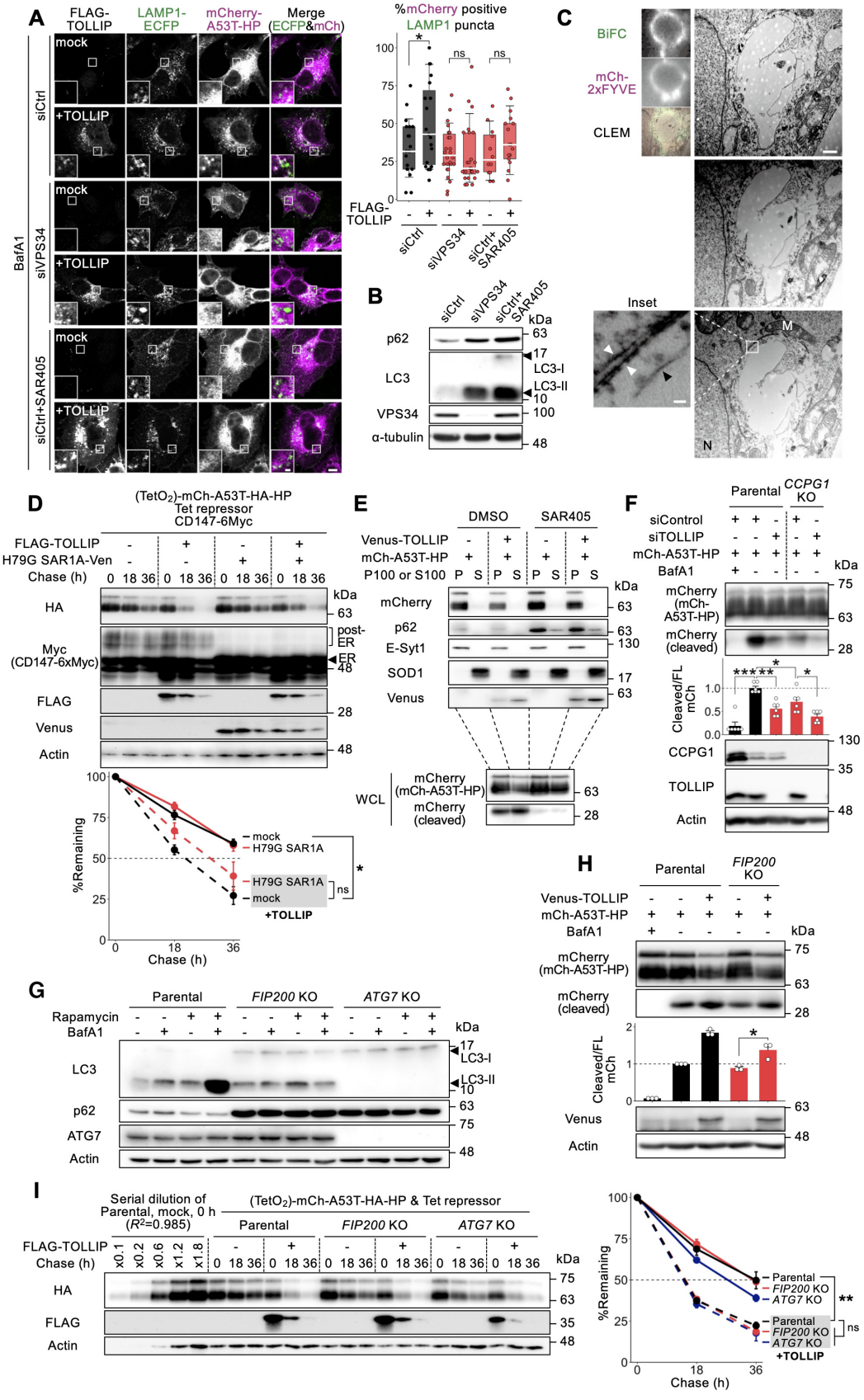

Figure EV3.

© 2023 The Authors

Figure EV4. TOLLIP clears disease-linked mutant membrane proteins.

A Turnover of VAPB variants monitored by promoter shut-off assay in HEK293A cells transfected with indicated siRNAs and HA-tagged VAPB variants as in Fig 7B. The graphs represent mean ± SEM of the turnover of mCherry-HA-VAPB protein quantified by immunoblotting ($n = 3$ independent experiments) and RNA quantified by real-time quantitative PCR in parallel experiments ($n = 2$ independent experiments). Statistical significance was determined at the final time point.

B, C Co-IP of HA-tagged P56S VAPB and N88S Seipin with Venus-TOLLIP variants in *TOLLIP*-KO HEK293A cells. Numerical data represent means of the relative amount of coimmunoprecipitated Venus-TOLLIP variants normalized to their expression levels in lysates ($n = 3$ independent experiments).

D Fractionation of HEK293A cells transfected with indicated constructs into 1% Triton X-100 soluble (S) and insoluble (P) fractions. The graphs represent mean ± SEM of the relative abundance of mCherry-tagged proteins in each fraction (left) and the expression level of BiP (right) ($n = 3$ independent experiments).

E Schematic representation of hypogonadotropic hypogonadism-linked E90K GnRHR (left) and lysosomal degradation of E90K GnRHR in HEK293A cells transfected with indicated constructs (right). The graph represents mean ± SEM of mCherry processing ($n = 3$ independent experiments).

F Turnover of Seipin-HA-mCherry transcripts quantified by real-time quantitative PCR conducted in parallel with the experiments in Fig 7B. The data are represented as mean ± SEM ($n = 2$ independent experiments).

Data information: $*P < 0.05$, $***P < 0.001$ by one-way ANOVA with Dunnett's multiple comparison test (E) or unpaired two-tailed Student's *t* test (A). †, presumed degradation products of Seipin.

© 2023 The Authors

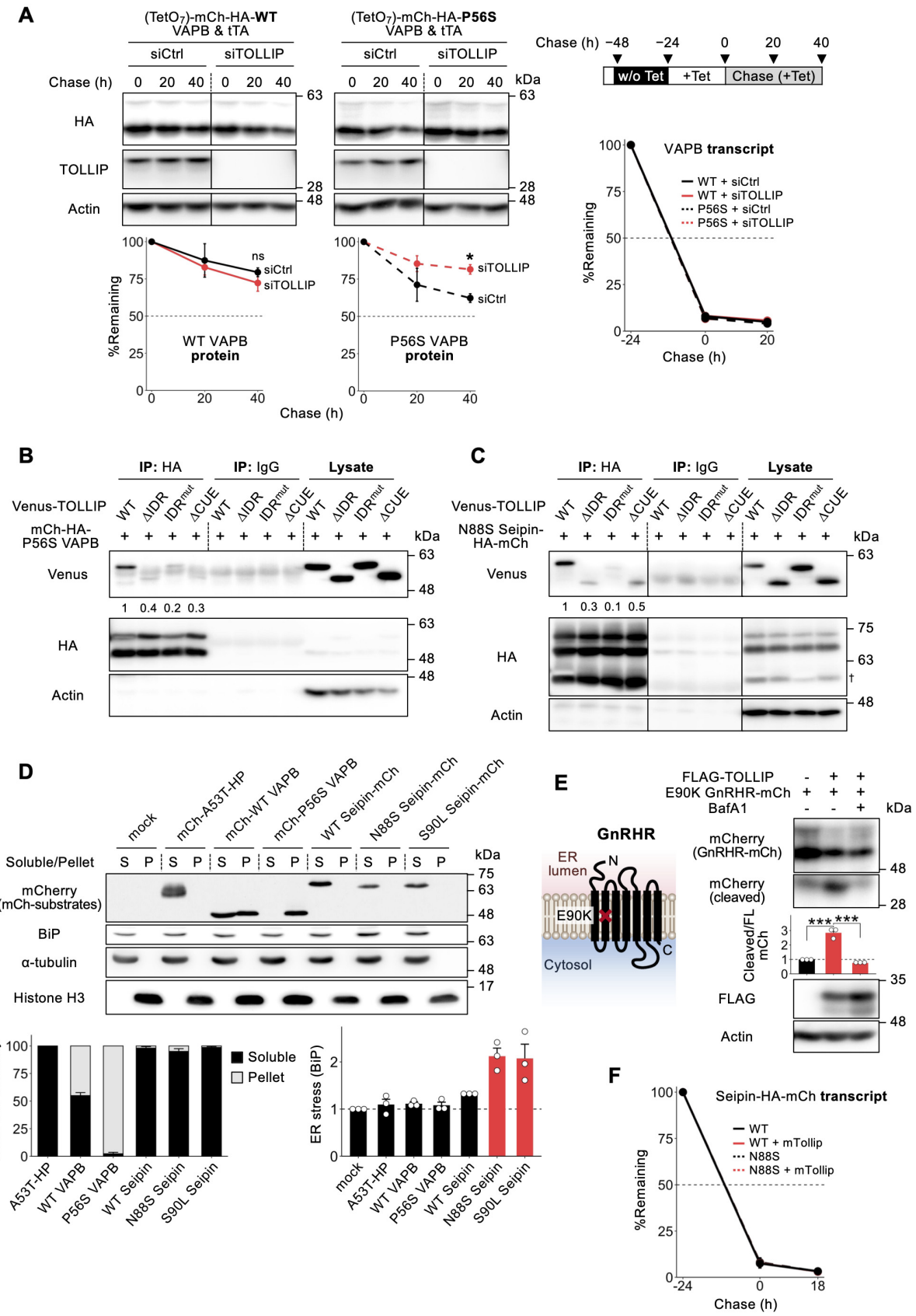

Figure EV4.

© 2023 The Authors

Figure EV5. TOLLIP suppresses ER stress after ERAD inhibition.

A Quantitative PCR of *BiP* (top) and semi-quantitative PCR of *XBP1* (bottom). Ctrl KO HEK293A cells were treated with increasing concentrations of EerI (5 or 20 μM), NMS-873 (1.5 or 15 μM), MG132 (0.8 or 10 μM), or Bort (80 or 2,000 nM) for 3 h. The graph represents mean ± SEM of the *BiP* level normalized to *RPS18*, and numerical data represent means of the relative *XBP1* mRNA splicing ($n = 3$ independent experiments).

B Immunoblot of indicated HEK293A cell lines transfected with HA-tagged null Hong Kong (NHK) variant of α1-antitrypsin and FLAG-tagged D18G transthyretin (TTR) and treated with 5 μM EerI for indicated times. The graph represents mean ± SEM of EerI-dependent fold increase in NHK and TTR levels normalized to α-tubulin ($n = 3$ independent experiments). These VCP-dependent luminal ERAD substrates accumulated to similar levels by EerI, suggesting that EerI treatment and subsequent blockade of ERAD were equally effective in all the cell lines analyzed.

C Immunoblot of indicated HEK293A cell lines treated with 5 μM EerI for indicated times. The graph represents mean ± SEM of the IRE1α level normalized to α-tubulin ($n = 4$ independent experiments). It had been previously shown that depletion of TOLLIP hyperactivated the ER stress sensor IRE1α and its downstream signaling in steady-state mouse embryonic fibroblasts (MEFs) by upregulating IRE1α protein (Pokatayev *et al*, 2020). However, *TOLLIP*-KO in HEK293A cells neither increased IRE1α nor activated steady-state downstream signaling. These results suggest that the role of TOLLIP as described herein is mechanistically different from the previously reported role in regulating the IRE1α signaling.

D Quantitative PCR of ER stress markers. Ctrl or *TOLLIP*-KO HEK293A cells were treated with 5 μM EerI for 48 h. The data are represented as mean ± SEM of ER stress marker levels normalized to *RPS18* ($n = 5$ independent experiments). $^{*}P < 0.05$, $^{***}P < 0.001$ by one-way ANOVA with Tukey's multiple comparison test.

E Schematic overview showing the TOLLIP-dependent selective lysosomal degradation of aberrant ER membrane proteins in relation to other reported ER quality control pathways.

© 2023 The Authors

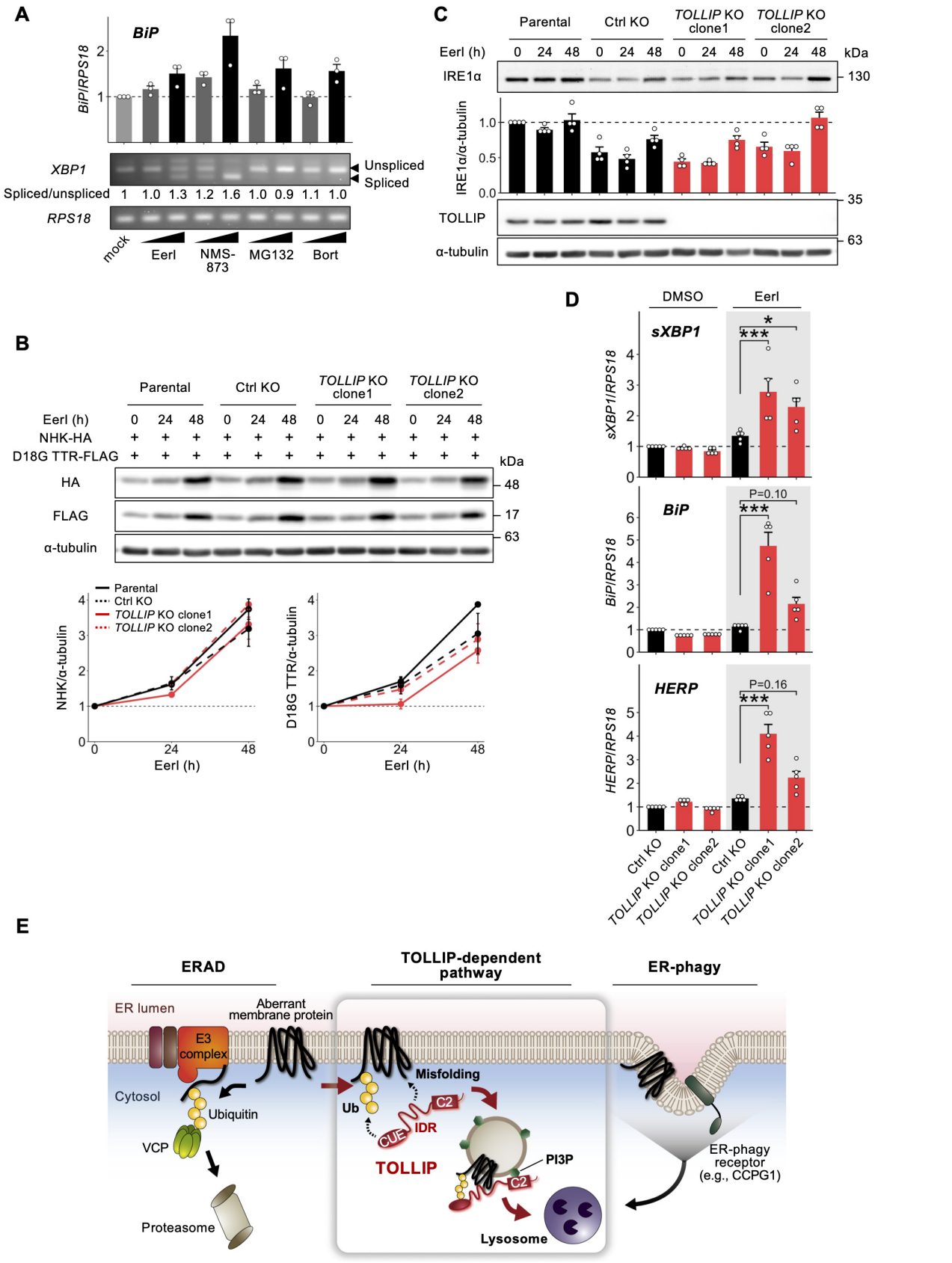

Figure EV5.

© 2023 The Authors